This paper describes objective technical results and analysis. Any subjective views or opinions that might be expressed in the paper do not necessarily represent the views of the U.S. Department of Energy or the United States Government.

SAND2021-7581C

Scaling of Reflected Shock Bifurcation at High Incident Mach Number

Kyle A. Daniel*, Kyle P. Lynch†, Charlie R. Downing ‡, Justin L. Wagner§
Sandia National Laboratories, Albuquerque, NM

Measurements of bifurcated reflected shocks over a wide range of incident shock Mach numbers, $2.9 < M_s < 9.4$, are carried out in Sandia's high temperature shock tube. The size of the non-uniform flow region associated with the bifurcation is measured using high speed schlieren imaging. Measurements of the bifurcation height are compared to historical data from literature. A correlation for the bifurcation height from Petersen et al. [1] is examined and found to over estimate the bifurcation height at $M_s > 6$. An improved correlation is introduced that can predict the bifurcation height over the range $2.15 < M_s < 9.4$ The time required for the bifurcation to pass over a stationary sensor is also examined. A non-dimensional time is introduced that collapses the data and yields a new correlation that predicts the temporal duration of the bifurcation.

I. Introduction

The shock tube is a versatile instrument used to create high temperature and pressure environments that are typically well described by 1-D shock relations. However, non-ideal effects may arise when a reflected shock interacts with the boundary layer included by the incident shock. In some cases, the reflected shock creates a strong adverse pressure gradient that the boundary layer cannot traverse, which forces the boundary layer to separate and the reflected shock to bifurcate.

This phenomena is called reflected shock bifurcation, which produces a region on non-uniform flow that negatively impact a variety of path integrated diagnostic techniques typically used in shock tubes. For example Bose et al. [2] compared absolute emission measurements of shock heated air in the Electric Arc Shock Tube (EAST) facility at NASA Ames Research with predictions from NEQAIR to assess the predictive capability of radiative heating codes like NEQAIR [3] and HARA [4]. NEQAIR was unable to predict the magnitude of broadband background radiation and consistently underpredicted the intensity of atomic lines. The authors hypothesized that molecules present in the lower temperature boundary layer may radiate as bands with low intensities over large wavelength ranges. Temperature and pressure non-uniformities induced by reflected shock bifurcation [5, 6] will also bias laser absorption-based diagnostics where the absorbing path length ideally needs to be highly uniform [7]. Other non-ideal effects related to reflected shock bifurcation include how the driver gas will bleed through the bifurcation when it interacts with the contact surface. This will contaminate the test gas and will reduce the effective test time in reflected shock tunnels [8, 9, 10].

Given the negative effect reflected shock bifurcation has on shock tube diagnostics and the test time concerns in reflected shock tunnels, the physics of reflected shock bifurcation has been studied extensively. A simplified model of the bifurcation first proposed by Mark [11] and later expanded on by Strehlow and Cohen [12], is shown in Fig. 1. Reflected shock bifurcation occurs when the boundary layer does not have enough momentum to be processed by the reflected shock. This occurs when the total pressure in the boundary layer is less than the post reflected shock pressure, i.e., $p_{0BL}/p_2 < p_5/p_2$. [11, 13]. For these cases the boundary layer collects in front of the reflected shock, forming a recirculation region defined by the area under line 0C in Fig. 1. An oblique shock 0A forms in front of the separated region and turns the fluid just outside of the boundary layer away from the wall. The fluid in region C0A is turned back parallel to the wall by a second oblique shock AC. The fluid processed by the reflected shock is approximately stagnant while the fluid moving through the trailing oblique shock has some finite velocity. The shear between these two layers forms a vortex sheet that starts at point A. These major features, namely the two oblique shocks that form the bifurcated 'foot' and the vortex sheet, are clearly observed in the color schlieren images of Kleine et al. [14].

A majority of of the flow non-uniformity associated with bifurcated reflected shocks occurs in the region defined by points 0-A-C-D in Fig. 1. The fluid in this region is comprised of a separated boundary layer (under line 0C)

*Postdoctoral Appointee, Member AIAA, kadani@sandia.gov
†Senior Member of the Technical Staff, Engineering Sciences Center, Member AIAA
‡Principal Technologist, Engineering Sciences Center
§Principal Member of the Technical Staff, Engineering Sciences Center, Associate Fellow AIAA, jwagner@sandia.gov

American Institute of Aeronautics and Astronautics
Sandia National Laboratories is a multimission laboratory managed and operated by National Technology & Engineering Solutions of Sandia, LLC, a wholly owned subsidiary of Honeywell International Inc., for the U.S. Department of Energy's National Nuclear Security Administration under contract DE-NA0003525.

and fluid that is processed by the leading oblique shock 0A. The fluid inside the separated flow region will have a different temperature, and thus chemical composition, compared to the centerline flow behind the reflected shock. This non-uniform flow region consequently has a large bias effect on shock tube diagnostic measurements behind reflected shocks.

Much of the literature concerning bifurcated reflected shocks focuses on describing the physics of the bifurcation and how to predict the conditions under which a bifurcated reflected shock will form [14, 15, 16, 17]. Only a small handful of studies, such as Petersen et al. [1], Davies and Wilson [9], Howard et al. [18], and Allen, [19], provide any quantitative measurement of the size and duration of the bifurcation and none examine reflected shock bifurcation at high incident shock Mach number ($M_s > 6$). The purpose of the current work is to examine bifurcated reflected shocks at high incident Mach number and to develop correlations that predict the size of the non-uniform flow zone. This is achieved using high speed schlieren imaging to measure the axial length of the bifurcation present on the shock tube window.

The remainder of this study is organized as follows: in section II, the shock tube facility and the measurement techniques are described in detail. Section III compares emission measurements from incident and bifurcated reflected shocks and present measurements of the bifurcation size over a large range of Mach numbers. These results are summarized in Section IV.

II. Experimental Methods

A. High Temperature Shock Tube Facility

The high temperature shock tube (HST) is a free-piston driven shock tube at Sandia National labs capable of producing strong shocks that generate simultaneous high pressure and temperature environments. The HST is similar to traditional shock tubes, where a shock wave is created when a diaphragm separating a driven and driver section at different pressures is burst. A key difference is the use of an 11.9 kg free-piston to isentropically compress the driver gas. This simultaneously pressurizes and heats the driver gas, allowing the generation of stronger shock waves compared to traditional shock tubes.

To generate these strong shocks, steel diaphragms of various thickness were burst using various helium-nitrogen mixtures as the driver gas and ambient temperature air as the driven gas air. To reduce the presence of water vapor the driven section was first pulled to vacuum and then backfilled with dry air. The facility is described in more detail in Lynch et al. [20].

Table 1. Flow Conditions

Case	M_s	M_r	T_2 (K)	T_5 (K)	p_2 (MPa)	p_5 (MPa)	ρ_2 (kg/m^3)	ρ_5 (kg/m^3)
1	8.12	2.70	3482	6230	0.57	4.70	0.55	2.48
2	8.36	2.92	3241	5180	0.61	5.57	0.64	3.32
3	9.37	3.08	3651	6155	0.77	7.78	0.70	3.74
4	5.07	2.48	1607	2828	0.11	0.74	0.23	0.90
5	6.29	2.60	2222	3593	0.13	1.00	0.20	0.93
6	5.97	2.59	2059	3593	1.48	11.21	2.51	10.74
7	6.07	2.60	2107	3665	1.53	11.61	2.52	10.88
8	2.91	2.08	750	1246	0.81	3.94	3.63	10.65
9	9.38	3.08	3652	6160	0.76	7.68	0.69	3.66
10	8.35	3.00	3059	4733	0.06	0.57	0.07	0.36
11	6.08	2.58	2112	3460	0.11	0.84	0.18	0.82
12	9.11	3.03	3574	5954	0.94	9.18	0.88	4.64

The pressure in driven section of the HST is monitored using fast response PCB pressure sensors (113B112). Sensors are provided an excitation voltage and amplified using a PCB model 483C signal conditioner. These voltages are low-pass filtered by using a Krohn-Hite Model 3384 with a four-pole butterworth filter with cutoff at 500 kHz. Data is recorded by an acquisition chassis equipped with a NI PXIe-6376 module that digitizes the signals at a sampling frequency of 2 MHz before being recorded on a personal computer via an in-house LabView code.

The various conditions examined in this study are shown in Table 1. Included in the table are the incident shock Mach number M_s, the reflected shock Mach number M_r, and post incident and reflected shock conditions for temperature (T_2, T_5), pressure, (p_2, p_5) and density, (ρ_2, ρ_5). Post shock conditions are calculated using the measured incident shock speed, as determined by shock crossing times given by the PCB sensors, and the initial driven conditions. These

values are used as inputs into standard shock tube relations [21] that include real gas effects and are calculated using the NASA Chemical Equilibrium with Applications (CEA) code [22].

Lastly note the bifurcation of the reflected shock is examined only in cases 1-11. Case 12 uses a short endwall to study the emission behind the incident shock and is compared to the emission behind the reflected shock in case 11. Through this comparison, the effect of the bifurcation on the emission intensity is examined as the ρ_5, T_5 in case 11 is nominally similar to ρ_2, T_2 in case 12.

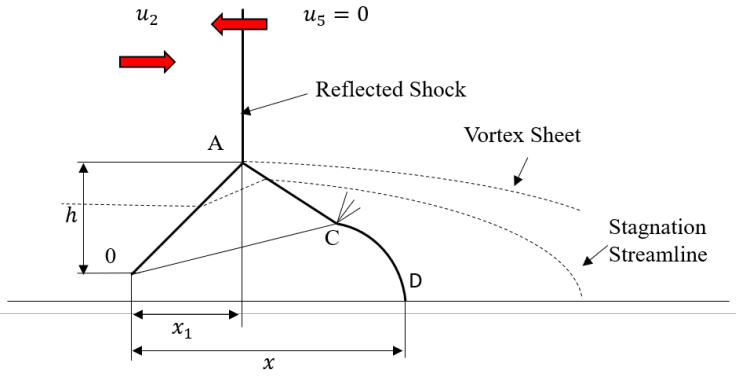

Figure 1. Model of a bifurcated reflected shock.

B. High-speed Schlieren Imaging

Visualization of the initial and reflected shock was captured using a lens schlieren system. The light source for the schlieren was a Cavilux Smart pulsed diode laser light having a wavelength of approximately 640 $\pm$ 10 nm and a pulse width of 10 ns. The light was collimated and focused onto the knife edge using two 101.6 mm plano-convex lenses placed on either side of the shock tube test section. A vertical knife edge was used to create schlieren images sensitive to the stream-wise density gradient. The images were recorded at 1 MHz and at a resolution of 250 x 400 pixels using a Shimadzu HPV-X2 high speed video camera. To avoid contaminating the schlieren images with light generated by the emission of shock heated air, a 640 ± 10 nm band pass filter and a polarizer were utilized. Schlieren images were spatially calibrated using a Edmond optics calibration dot target with 0.5 mm spacing.

C. Low Dispersion Spectrometer

A high-speed, low dispersion spectrometer was used in this study to broadly capture the visible wavelength regime. The emission from the shock heated air was collected using a 2 mm reflected collimator and a 105-micron diameter round-to-linear fiber bundle from Thorlabs (BFL105HS02), where the linear end was aligned parallel with the spectrometer slit. To ease alignment of the collection optics to the moving HST, a custom mount was attached to the test section.

Light collected from the fiber bundle was passed through the spectrometer slit and then collimated with a Nikon 105 mm lens onto a Thorlabs visible transmission grating with 300 grooves per mm (model GT50-3). Light then passed through a Thorlabs 500 nm long-pass filter (FEL0500) to prevent spectral overlap. An additional 105 mm lens focused the light out of the long pass filter onto the sensor of a Photron Fastcam SA-Z camera used to collect emission images. The system was operated at a framing rate of 200 kHz at a spatial resolution of 1024 × 16 pixels. Special care was taken to maximize the dynamic range of the instrument without saturating the detector.

D. Absolute Emission Spectroscopy

The low dispersion spectrometer was calibrated for both wavelength and absolute spectral irradiance. The wavelength calibration was performed with an Ocean Optics HG-2 Mercury-Argon wavelength calibration source that provided multiple strong emission lines over a range of 250 to 920 nm. During calibration, the round end of the fiber bundle was connected directly to the wavelength calibration source via an SMA connection. Wavelength calibration images were collected with an exposure of 1000 μs, a framerate of $60 Hz$, and a resolution of 1024 by 16 pixels. An identical resolution was also used for black body calibration and HST emission measurements. The transformation from pixel

to wavelength space was performed by first identifying the wavelength of strong spectral peaks in the calibration image. The wavelength space of the calibration image was then determined by linearly interpolating between the wavelengths of the identified peaks. The spectral resolution of the low dispersion spectrometer was evaluated using the full width half max (FWHM) of each emission line in the calibration. The resulting spectral resolution was determined to be about 4 nm. To obtain an absolute spectral emission measurement, the sensitivity of the entire optical system must be accounted for. A system response function that includes the sensitivity of the camera, spectrometer, and window geometry is determined by ratioing the measured intensity of a black body calibration source with the spectral irradiance of an ideal black body at the same temperature. Here we define the system response function as,

$$f(\lambda) = \frac{I_m(\lambda)}{I_p(\lambda, T)}, \tag{1}$$

where $I_m(\lambda)$ is the measured intensity of the black body calibration source, calculated as the summed pixel intensity from each column in the calibration image. The spectral irradiance of an ideal black body, $I_p(\lambda, T)$, is described by Plank's law as

$$I_p(\lambda, T) = \frac{2\pi hc^2}{\lambda^5} \frac{1}{\exp(\frac{hc}{\lambda kT}) - 1}, \tag{2}$$

where h is Planck's constant, c is the speed of light, k is Boltzmann's constant, and T is the temperature of the black body emitter. The black body calibration source used was an Infrared System IR-564 black body set at a temperature of 1200 C, the maximum temperature of the system. Calibration images were again taken with the Fastcam SA-Z set at an exposure of 1000 μs , a framerate of $60Hz$, and resolution of 1024 by 16 pixels. Further, black body calibrations were performed using the fiber mounting system and the window port of the shock tube. The inclusion of the window port in the calibration directly accounts for variations in spectral intensity due to losses through the window and ensures the calibration accounts for the sensitivity of the entire optical system.

With the system response function known, the absolute spectral emission can be determined by correcting the measured intensity as,

$$I_c(\lambda) = \frac{I_E(\lambda)}{f(\lambda, T)} \frac{\epsilon_m}{\epsilon_E}, \tag{3}$$

where $I_c(\lambda)$ is the corrected absolute spectral emission, $I_E(\lambda)$ is the summed pixel intensity of each column in an emission image, ϵ_m is the exposure time used in the emission image, and ϵ_E is the exposure time used in the black body calibration image. Note that at very low exposure times, the variation in image intensity with exposure time is not linear (i.e., a doubling of exposure time does not result in a doubling of the collected light). To account for the non-linearities associated with the low exposure times used in the HST emission measurements, a correction is applied to the exposure ratio. This correction is found by measuring these non-linearities directly through calibration measurements of an Ocean Optics HL-2000 halogen light source at varying exposure times.

III. Results & Discussion

A. Emission from Bifurcated Reflected Shocks

The impact of a bifurcated reflected shock on a path integrated measurement is evaluated by comparing the emission behind an incident and reflected shock with similar density and temperature. The emission from shock heated gas is well known to scale linearly with density and to the fourth power with temperature. Therefore, the emission from gas behind reflected and incident shocks with similar density and temperature will have a comparable absolute spectral irradiance. An incident shock has no bifurcation, so a comparison to a bifurcated reflected shock will demonstrate the effect the bifurcation has on the emission intensity and the temporal duration of the non-uniformity.

A contour plot of the emission behind an incident shock (case 12) is compared to a reflected shock (case 11) in Fig. 2. In both contour plots time zero represents the first emission frame where the signal is above the noise level. The contour intensity is the logarithm of the absolute emission intensity normalized by the maximum intensity in the wavelength-time space shown. Note because the emission intensity is absolute, values from each case can be directly compared.

For the incident shock case in Fig. 2a there is a step increase in the emission intensity. Comparatively, the emission in the reflected shock case in Fig. 2b increases over multiple frames until it reaches a steady state value. This slow increase in emission intensity is caused by the temperature and density of the fluid in the bifurcation region that biases the emission measurement to a lower intensity.

This biasing effect is more clearly observed in Fig. 2c, which plots $I_{\text{reflected}}/I_{\text{incident}}$, the ratio of the reflected to incident emission intensity that is summed over the wavelength range 500-750 nm. Moving forward from time 0, the emission intensity ratio $I_{\text{reflected}}/I_{\text{incident}}$ increases monotonically for $\approx$25 μs until the reflected and incident emission intensities are about equal. In the reflect shock case this time represents when the bifurcation has passed through the measurement volume and emission is being collected from uniformly heated gas.

Emission measurements behind reflected shocks will be biased to lower values while the bifurcation region, defined by points 0-A-C-D in Fig. 1, is within the measurement volume. The magnitude of the biasing effect is a function of the height of the bifurcation h and the temperature and density of the fluid in region 0-A-C-D. The time it takes for this non-uniform flow region to leave the measurement volume, defined as Δt_{0D}, is a function of the length of the bifurcation region x and the reflected shock speed.

Without the comparison to an incident shock case, an estimate Δt_{0D} and the magnitude of the biasing effect is not always obvious from emission measurements behind the reflected shock. Further, wall pressure traces do not add much information either, as the pressure inside the bifurcation region is relatively constant. These observations motivate the rest of the study, which aims to characterize reflected shock bifurcation at high incident Mach number to better understand its impact on path integrated diagnostics.

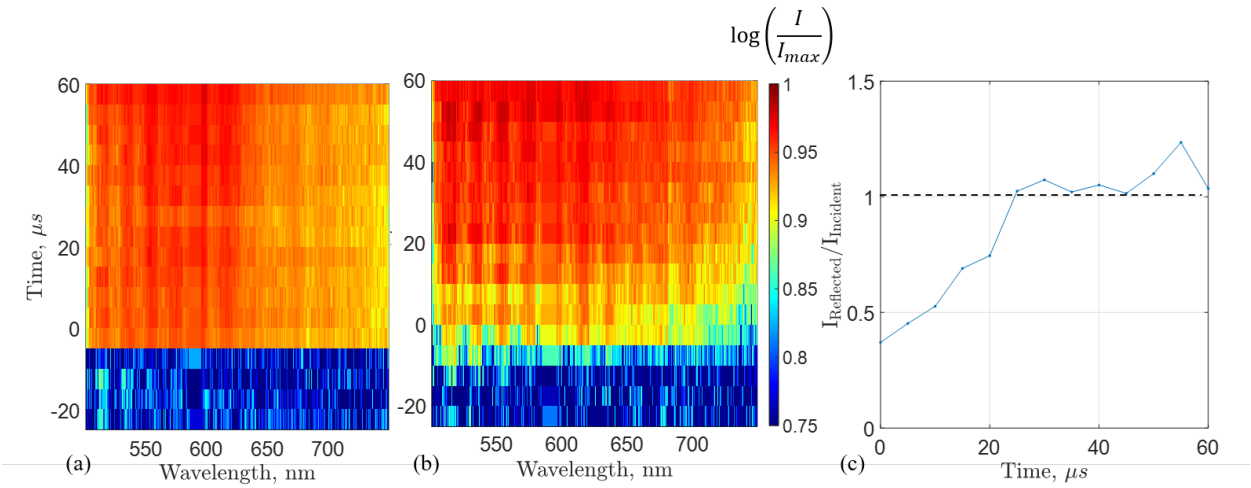

Figure 2. (a) Emission contour behind the incident and (b) reflected shock. (c) Ratio of reflected shock to incident shock emission.

B. Measurement of Reflected Shock Bifurcation

The impact the bifurcation region will have on a diagnostic can be quantified by the total height of the bifurcation h and the angle of the leading oblique shock θ. With knowledge of θ, the fluid state inside the bifurcation region can be estimated using oblique shock relations. This information, along with h can then allow a rough profile of the temperature or density across the test section to be determined.

The height of the bifurcation can be estimated using the procedure outline in Mark [11]. Starting in shock fixed coordinates the boundary layer Mach number M_{BL} can be calculated as,

$$M_{BL} = \frac{2(\gamma_1 - 1)M_s^2 + 3}{(\gamma_1 + 1)M_s}. \tag{4}$$

With the boundary layer Mach number known, the total pressure ratio in the boundary layer $\frac{p_{0,BL}}{p_2}$ is found using isentropic relations or the Rayleigh pitot formula depending whether M_{BL} is supersonic,

$$\begin{aligned} M_{BL} < 1 : \frac{P_{0,BL}}{p_2} &= \left[1 + \frac{\gamma - 1}{2} M_{BL}^2\right]^{\gamma/(\gamma-1)} \\ M_{BL} > 1 : \frac{p_{0,BL}}{p_2} &= \left[\frac{\gamma - 1}{2} M_{BL}^2\right]^{\gamma/(\gamma-1)} \times \left[\frac{2\gamma}{\gamma+1} M_{BL}^2 - \frac{\gamma - 1}{\gamma + 1}\right]^{1/(1-\gamma)} \end{aligned} \tag{5}$$

A key assumption in the Mark [11] model is the pressure inside the bifurcation zone is constant and equal to the stagnation pressure in the boundary layer. With this simplification the angle of the leading shock foot θ can be calculated using oblique shock relations,

$$M_R^2 \sin^2\theta = \frac{(\gamma+1)\frac{p_{0,BL}}{p_2} + \gamma - 1}{2\gamma}. \tag{6}$$

Mark [11] as well as others in the literature [9, 12] have shown this assumption to be accurate for a range of incident Mach numbers. The height of the bifurcated region h can then be found through geometry as,

$$h = x_1 \tan\theta \tag{7}$$

With knowledge of the shock speed and initial conditions (ie., M_s, M_r), and a measurement of the distance from the leading edge of the bifurcation to the reflected shock x_1, the height of the bifurcation can be found.

The length x_1 can be measured directly using schlieren images of the bifurcated reflected shock. Example schlieren images in Fig. 3a show the incident shock moving right towards the endwall. The reflected shock forms in Fig. 3b where the dark strip represents the center of the reflected shock and the turbulent region upstream represents the leading portion of the shock foot, i.e., section 0-A. The turbulent region downstream of the reflected shock center is the trailing half of the shock foot. This region, section A-D, marks the end of the bifurcation. Images of later times when the reflected shock moves away from the endwall are shown in Fig. 3c-d. Here the length, as well as the height, of the bifurcation grows with distance from the endwall.

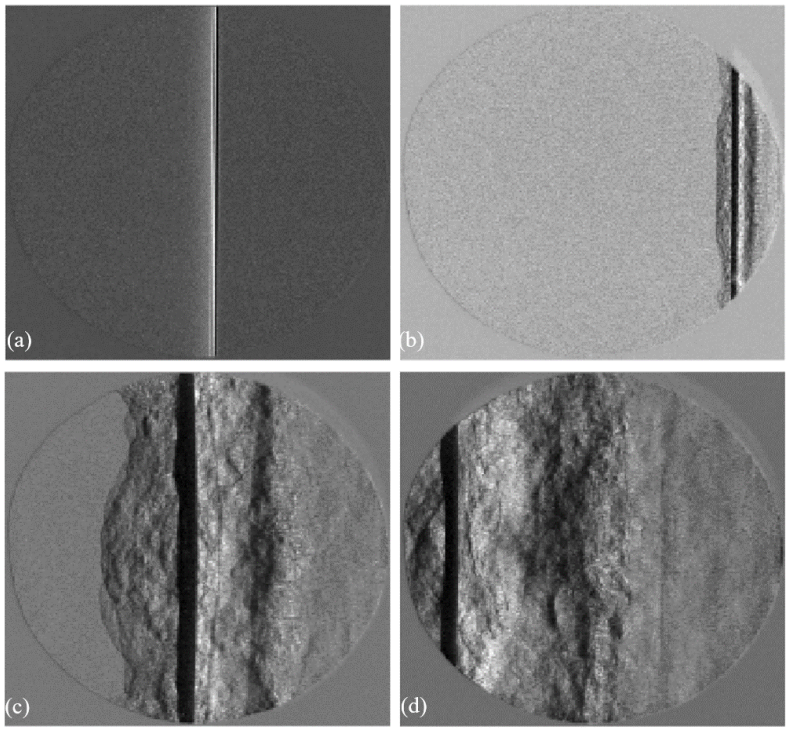

Figure 3. Schlieren images of the (a) incident shock and (b)-(d) reflected shock.

The distance x_1 can be extracted from schlieren images using simple image processing techniques. A band of pixels in the center of the schlieren image is vertically binned to form the x-t diagram in Fig. 4. Here the bottom line that runs left to right is the incident shock that reflects off the endwall located at $x = 0$. The center of the reflected shock along with the leading and trailing edges of the bifurcation region are clearly observed in the x-t diagram. The length x_1 is extracted from the x-t diagram by measuring the distance along the horizontal line marked in Fig. 4. The total time it takes the bifurcation to pass over a stationary sensor located a known distance from the endwall Δt_{0D} can also be determined using the distance along the vertical line marked in Fig. 4.

Using the x-t diagrams of schlieren images, the distance x_1, the height of the bifurcation h, and the time Δt_{0D} can be measured for each case as a function of distance from the endwall. These values and how they vary with M_s are examined in the next section.

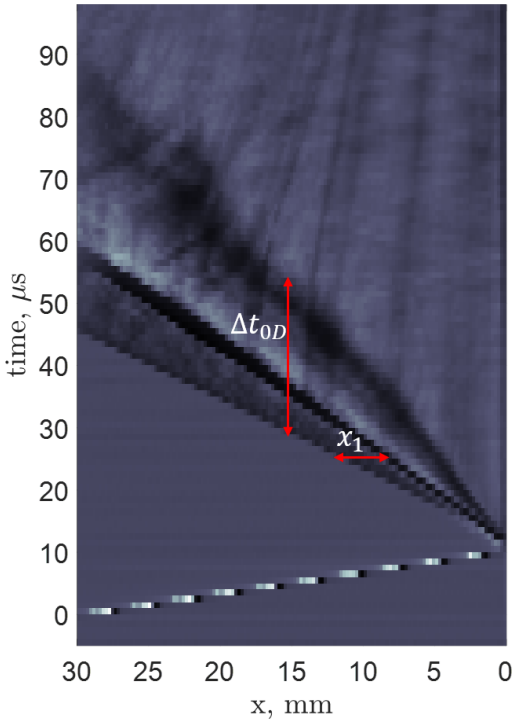

Figure 4. x-t diagram of incident and reflect shocks. Included are markings for x_1, the length of the bifurcation leading edge and Δt_{0D}, the time required for the bifurcation region to pass over a stationary sensor.

C. Correlations for Bifurcation Height and Duration

Using the methods described in the previous section, the height of the bifurcation h and the time it takes the bifurcation to pass over a stationary sensor Δt_{0D} are measured. For cases 1-11 the height of the bifurcation is normalized by distance from the endwall and plotted as a function of M_s in Fig. 5a. Included are measurements of the bifurcation height taken from the literature, where air or nitrogen was the test gas. Note that to the authors knowledge this is the first paper since Davies et al. [9] to compare measurements of the bifurcation height from multiple studies.

As shown in Fig.5a, the height of the bifurcation generally increases with incident Mach number. This trend can be captured by a simple correlation as was done by Petersen et al.[1]. The authors developed a correlation for the bifurcation height using a set of data that included a wide range of reflected shock pressure ($0.8MPa < p_5 < 11.9MPa$) and test gas that included various mixtures of nitrogen, oxygen, methane, carbon dioxide, helium, and argon. However, the authors only examined a limited range of incident shock Mach number, namely $2.5 < M_s < 4.4$. The correlation for bifurcation height from Petersen et al. [1] took the form,

$$h = 7.5 M_s^{1.07} \gamma_2^{-2.66} \bar{M}^{-0.37}, \tag{8}$$

where $\bar{M}$ is the molecular weight of the test gas and the height h is in mm.

The Petersen et al. [1] correlation is evaluated against the current data and the data from the literature in Fig. 5b. Here the x-axis is the height predicted using Eq. (8) and the black line represents a perfect match between the correlation and measurement. For low Mach numbers the Petersen et al. [1] correlation predicts bifurcation height fairly well, but begins to deviate as the Mach number is increased. This trend is not surprising as the correlation was only developed with $M_s < 4.4$.

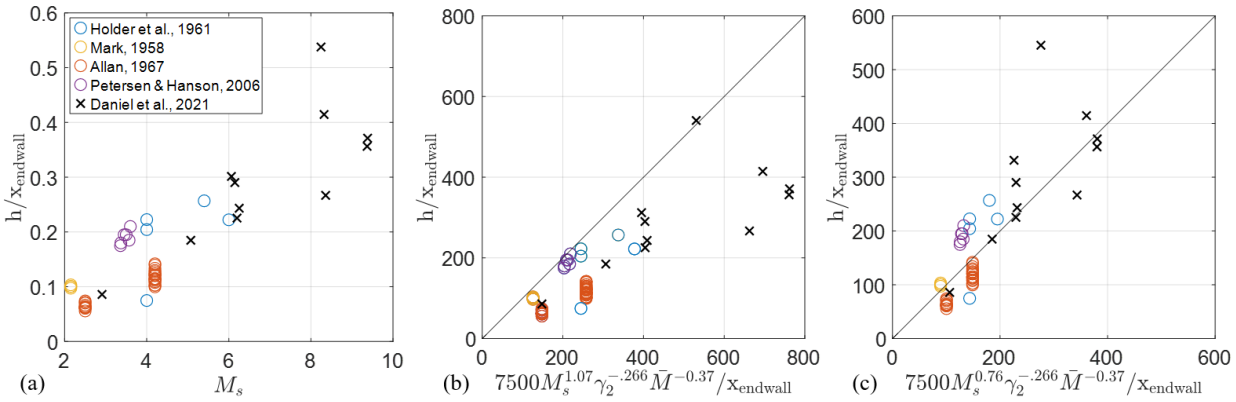

Figure 5. (a) The bifurcation height h as a function of incident mach number. (b) The Petersen et al. [1] for the bifurcation height. (c) improved correlation for the bifurcation height.

The high Mach number data in the current study can be used to improve the Petersen et al. [1] correlation by changing the power on the Mach number term in Eq. (8). Using a least squares fit to the current data, as well as all historical data shown, an improved correlation is developed,

$$h = 7.5 M_s^{0.76} \gamma_2^{-2.66} \bar{M}^{-0.37}. \tag{9}$$

The new correlation is evaluated in Fig. 5c where the x-axis the is the bifurcation height estimated using Eq. (9). Here the correlation produces a better fit to the data, especially at higher Mach number and can be used to predict the bifurcation height for Mach numbers up to 9.38. Note the correlation has only been tested with air or nitrogen as the test gases. In future work the bifurcation of the reflected shock at high Mach number will be examined in different test gases to examine the effect of γ_2, and $\bar{M}$.

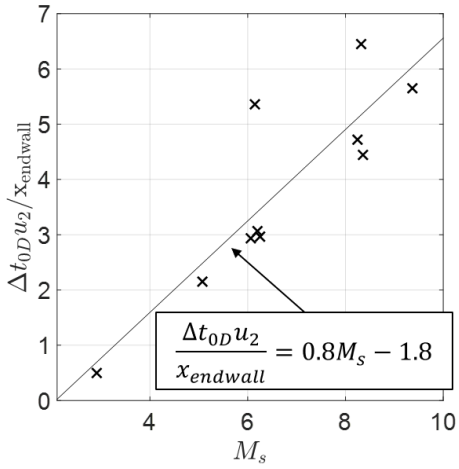

Figure 6. (a) The time it takes the bifurcation region to pass over a stationary sensor, Δt_{0A} as a function of incident mach number.

A correlation can also be developed to predict the time it takes the bifurcation region to pass over a stationary sensor, Δt_{0D}. Measurements for Δt_{0D} from cases 1-11 are normalized using the induced velocity behind the incident shock u_2 and the distance to the endwallx_{endwall}. This dimensionless quantity is plotted as a function of M_s in Fig. 6. Here the normalization works well, collapsing the data along a line that can be linearly fit as a function of M_s. A

linear fit of the data in Fig. 6 yields the following correlation,

$$\frac{\Delta t_{0D} u_2}{x_{\text{endwall}}} = 0.8 M_s - 1.8. \tag{10}$$

The correlation for Δt_{0D} is plotted as the solid line in Fig. 6 and shown to predict the bifurcation duration with moderate accuracy over a wide range of Mach numbers. This correlation is useful when used in conjunction with a pressure trace during a shock tube experiment. The pressure trace can easily identify the start of the bifurcation, when the pressure first rises across the leading oblique shock, but cannot easily identify the exact time the bifurcation region has fully passes over the sensor. When the pressure trace is used with the correlation in Eq. (10), it can inform a diagnostic technique when the non-uniform flow region has passed out of the measurement volume. Improvements can still be made to the correlation for Δt_{0D} by accounting for different test gases and incorporating γ_2 and $\bar{M}$ into the correlation. This is a topic for future work.

IV. Conclusion

High speed schlieren measurements were made in Sandia's high temperature shock tube to measure reflected shock bifurcation over a large range of incident shock Mach numbers ($2.9 < M_s < 9.4$). The bifurcation height was measured and compared to a set of historical data from the literature. A correlation from Petersen et al. [1] that estimates the bifurcation height was evaluated using the current data and the historical data. The correlation was found adequately estimate the bifurcation height at low Mach number and under under predict it as the Mach number increased. An improved correlation was introduced that modifies the Petersen et al. [1] correlation and was found to adequately predict bifurcation height over the range $2.15 < M_s < 9.4$.

Measurements for the time required for the bifurcation region to pass over a stationary sensor, Δt_{0D} are also shown. Normalizing the time Δt_{0D} using the induced velocity behind the incident shock and the distance from the endwall was found to favorably collapse the data. Using this non-dimensionalization a linear fit was applied to yield a correlation to predict Δt_{0D}.

The data presented in this study have helped develop correlations that can predict the size and duration of reflected shock bifurcation over a large range of incident shock Mach numbers. These correlations are useful in how they can be used to understand the impact the bifurcation will have on path integrated diagnostics and give an estimate of the time required for the bifurcation region to pass through a sensor measurement volume.

Improvements can be made to the these correlations by extending them to different test gases. Currently, these correlations have only been shown for cases where air or nitrogen are the test gas. A topic for future work includes making measurements of bifurcated reflected shocks in a range test gases and incorporating the effect of specific heat ratio and molecular weight into the correlations.

Acknowledgments

Sandia National Laboratories is a multi-mission laboratory managed and operated by National Technology & Engineering Solutions of Sandia, LLC, a wholly owned subsidiary of Honeywell International Inc., for the U.S. Department of Energy's National Nuclear Security Administration under contract DE-NA0003525. This paper describes objective technical results and analysis. Any subjective views or opinions that might be expressed in the paper do not necessarily represent the views of the U.S. Department of Energy or the United States Government.

This work is supported by the Laboratory Directed Research and Development (LDRD) program at Sandia National Laboratories.

References

[1] Petersen, E. and Hanson, R., "Measurement of reflected-shock bifurcation over a wide range of gas composition and pressure," *Shock Waves*, Vol. 15, No. 5, 2006, pp. 333–340.

[2] Bose, D., McCorkle, E., Bogdanoff, D., and Allen, G., "Comparisons of air radiation model with shock tube measurements," *47th AIAA Aerospace Sciences Meeting Including The New Horizons Forum and Aerospace Exposition*, 2009, p. 1030.

[3] Whiting, E. E., Park, C., Liu, Y., Arnold, J. O., and Paterson, J. A., "NEQAIR96, Nonequilibrium and Equilibrium Radiative Transport and Spectra Program: User's Manual," 1996.

[4] Johnston, C. O., *Nonequilibrium shock-layer radiative heating for Earth and Titan entry*, Ph.D. thesis, Virginia Tech, 2006.

[5] Hargis, J. W. and Petersen, E. L., "Shock-tube boundary-layer effects on reflected-shock conditions with and without Co 2," *AIAA journal*, Vol. 55, No. 3, 2017, pp. 902–912.

[6] Petersen, E. L. and Hanson, R. K., "Nonideal effects behind reflected shock waves in a high-pressure shock tube," *Shock Waves*, Vol. 10, No. 6, 2001, pp. 405–420.

[7] Girard, J. and Hanson, R., "Minimally intrusive optical probe for in situ shock tube measurements of temperature and species via tunable IR laser absorption," *Applied Physics B*, Vol. 123, No. 11, 2017, pp. 1–11.

[8] Bull, D. and Edwards, D., "An investigation of the reflected shock interaction process in a shock tube." *AIAA Journal*, Vol. 6, No. 8, 1968, pp. 1549–1555.

[9] Davies, L. and Wilson, J., "Influence of Reflected Shock and Boundary-Layer Interaction on Shock-Tube Flows," *The Physics of Fluids*, Vol. 12, No. 5, 1969, pp. I–37.

[10] Dumitrescu, L., Popescu, C., and Brun, R., "Experimental studies of the shock reflection and interaction in a shock tube," *Shock Tubes*, University of Toronto Press, 1970, pp. 751–770.

[11] Mark, H., *The interaction of a reflected shock wave with the boundary layer in a shock tube*, National Advisory Committee for Aeronautics, 1958.

[12] Strehlow, R. A. and Cohen, A., "Limitations of the reflected shock technique for studying fast chemical reactions and its application to the observation of relaxation in nitrogen and oxygen," *The Journal of Chemical Physics*, Vol. 30, No. 1, 1959, pp. 257–265.

[13] Byron, S. and Rott, N., "On the interaction of the reflected shock wave with the laminar boundary layer on the shock tube walls," *Proceedings of the 1961 Heat Transfer and Fluid Mechanics Institute*, Vol. 38, Stanford Univ. Press Stanford, 1961, p. 54.

[14] Kleine, H., Lyakhov, V., Gvozdeva, L., and Grönig, H., "Bifurcation of a reflected shock wave in a shock tube," *Shock Waves*, Springer, 1992, pp. 261–266.

[15] Wilson, G., Sharma, S., and Gillespie, W., "Time-dependent simulation of reflected-shock/boundary layer interaction in shock tubes," *Shock Waves@ Marseille I*, Springer, 1995, pp. 439–444.

[16] NISHIDA, M. and Min-gyoo, L., "Reflected-shock/side-boundary-layer interaction in a shock tube," *Album of visualization*, Vol. 13, 1996, pp. 1–2.

[17] Daru, V., Fernandez, G., and Tenaud, C., "On CFD to investigate bifurcated shock wave pattern," *Proceedings of the 21st International Symposium on Shock Waves Australia, Panther Publishing and Printing, Fyshwick*, 1997, pp. 1091–1097.

[18] Holder, D., Stuart, C., and North, R., "The interaction of a reflected shock with the contact surface and boundary layer in a shock tube," Tech. rep., AERONAUTICAL RESEARCH COUNCIL LONDON (UNITED KINGDOM) Report No. 22 891, 1961.

[19] Allan, W., Ph.D. thesis, Univeristy of Southampton England, 1967.

[20] Lynch, K. P. and Wagner, J. L., "A free-piston driven shock tube for generating extreme aerodynamic environments," *AIAA Scitech 2019 Forum*, 2019, p. 1942.

[21] Anderson, J. D., *Modern compressible flow: With Historical Perspective*, McGraw-Hill Education, 2003.

[22] "NASA. [Online]. Available: https://www.grc.nasa.gov/www/CEAWeb/ceaHome.htm," .